Comprehensive Ventilation/Perfusion SPECT

John Palmer, Ulrika Bitzén, Björn Jonson, and Marika Bajc

Departments of Radiation Physics and Clinical Physiology, Lund University Hospital, Lund, Sweden

Lung scintigraphy is the primary tool for diagnostics of pulmonary embolism. A perfusion study is often complemented by a ventilation study. Intermediate probability scans are frequent. Our goal was to develop a fast method for tomographic ventilation and perfusion scintigraphy to improve the diagnostic value of lung scintigraphy. **Methods:** SPECT was performed with a dual-head gamma camera. Acquisition parameters were determined using a thorax phantom. Ventilation tomography after inhalation of 30 MBq ^{99m}Tc-diethylenetriaminepentaacetate (DTPA) aerosol was, without patient movement, followed by perfusion tomography after an intravenous injection of 100 MBq ^{99m}Tc-labeled macroaggregated albumin (MAA). Total SPECT acquisition time was 20 min. ^{99m}Tc-DTPA clearance, calculated from initial and final SPECT projections, was used for correction of the ventilation projection set before iterative reconstruction of ventilation and perfusion. The ventilation background was subtracted from the perfusion tomograms. A normalized ventilation/perfusion quotient (V/P quotient) image set was calculated. The method was evaluated on a trial group of 15 patients. **Results:** Ventilation and perfusion images had adequate quality and showed ventilation/perfusion (V/Q quotient) relationships more clearly than did planar images. Frontal and sagittal slices were superior to planar scintigraphy for characterization of embolized areas. The V/Q quotient was supportive, particularly in the patients with chronic obstructive pulmonary disease. **Conclusion:** Fast, high-quality, ventilation/perfusion SPECT with standard isotopes doses is feasible and may contribute to higher objectivity in evaluating lung embolism as well as other lung diseases. The costs for the procedure and patient care until diagnosis are low because of the comprehensive system for the study and, particularly, the short time for its completion.

Key Words: lung; ventilation; perfusion; lung embolism; tomography

J Nucl Med 2001; 42:1288–1294

Pulmonary embolism is a common condition with a high mortality in untreated patients (*1*). Early diagnosis is essential to decrease mortality (*2*,*3*). Because of its noninvasive character, pulmonary scintigraphy is a preferred diagnostic method, if available (*4*). In principle, the diagnosis of lung embolism is based on perfusion defects. A ventilation scan is useful to distinguish between perfusion defects of different nature. Intermediate probability scans are frequent (*5*–*8*). Although SPECT has been advocated previously for lung scintigraphy (*9*), it is commonly performed using planar technique. Ventilation is often performed as an adjunct to perfusion only if the perfusion scan so indicates. Such an approach appears to be superficially advantageous. Time gained by avoiding ventilation studies in some patients may be offset by time lost in decision making and prolonged patient handling. If ventilation is performed much later than perfusion, the quality of the study as a whole will suffer. Further degradation of mismatch evaluation is introduced by repositioning the patient for the ventilation study. Work by Corbus et al. (*8*) suggests that SPECT can improve specificity and significantly decrease the number of intermediate probability results. Magnussen et al. (*10*) found that the mediobasal segment of the right lung was much better visualized with SPECT than with planar scintigraphy. The lung bases are a common site for lung emboli. Although spiral CT may have a high sensitivity and specificity for central embolism (*11*,*12*), it has limitations for peripheral embolus locations (*7*). Our objective was to develop a low-cost, efficient clinical method for high-quality ventilation and perfusion tomography. Thus, 2 SPECT studies with identical orbits, ventilation and perfusion, were performed in succession with the patient immobile. We describe a new way of presenting the data as a ventilation/perfusion quotient (V/P quotient). To fulfill the clinical demands for efficiency, the whole procedure should be completed within 30 min. Further studies would be needed to conclusively determine whether the method improves the diagnostic power of lung scintigraphy.

MATERIALS AND METHODS

SPECT Acquisition Parameters

A large field-of-view, dual-head gamma camera was used (DST-Xli; SMV, Buc, France). The prerequisite was that the entire study be completed within 30 min using a patient dose similar to that of planar scintigraphy. Under these conditions, immobilization during the 2 consecutive SPECT scans will be well tolerated by the patient. Acquisition parameters were evaluated using an in-house–constructed Perspex thorax phantom, with heart and spine inserts. The lungs were simulated by damp cork of density 0.3 g/cm^3. To produce a fairly homogeneous lung substitute, the cork was sprayed with a solution of ^{99m}Tc before filling the phantom. Cylindric plastic inserts, filled with inactive cork and of dimensions 2×5.5 and 3×7.5 cm (diameter $\times$ length), were used to simulate emboli. A low-energy, high-resolution collimator and a low-energy, all-purpose collimator, matrix 64×64 and 128×128, and 4 different total count numbers were tested in the combinations

Received Nov. 27, 2000; revision accepted Apr. 9, 2001.

For correspondence or reprints contact: Marika Bajc, MD, PhD, Department of Clinical Physiology, Lund University Hospital, S-221 85 Lund, Sweden.

TABLE 1
Basic Acquisition Configurations Evaluated Using Thorax Phantom

Collimator	64 × 64 matrix (128 projections/360°)		128 × 128 matrix (256 projections/360°)	
	Counts × 10^6	Locations seen	Counts × 10^6	Locations seen
All purpose	1.5	10	—	—
	2.9	16	3.2	16
	5.6	**19**	6.2	17
	10.8	19	12.0	**19**
High resolution	0.7	7	—	—
	1.3	12	1.5	13
	2.6	**18**	2.9	15
	4.9	18	5.5	**23**

Total acquired counts and resulting perceptibility in terms of number of emboli locations seen for different collimators and matrix sizes. Level up to which additional counts resulted in improved perceptibility are indicated in boldface type.

shown in Table 1. The pixel size was 6.8 mm in a 64 × 64 matrix and 3.4 mm in a 128 × 128 matrix. The slices recorded in the 128 × 128 matrix were added 2 by 2 to create slices of thickness similar to that obtained with the smaller matrix. An experienced reader of scintigrams judged from all slices in how many locations the "emboli" were observed.

Disposition of Acquisition Times and Activities

In the patient studies, ventilation was studied before perfusion because (a) this facilitates determination of the lung clearance of ^{99m}Tc-diethylenetriaminepentaacetate (DTPA) and (b) the higher activity, necessary for the second part of the study, gives an improved delineation of perfusion defects that is required for diagnosis of lung embolism. With total scanning time and total administered activity limited to fixed values, the disposition of acquisition times and activities for the 2 scans should be chosen with care. A guideline can be obtained from an expression for the estimated statistical error of the calculated V/P quotient, as follows. The derivation assumes Poisson statistics and, thus, is strictly valid only if the V/P quotient is to be calculated from projection images rather that from reconstructed data. However, contrary to filtered backprojection, the maximum-likelihood expectation maximization algorithm (from which ordered-subsets expectation maximization [OSEM] was developed for computational efficiency) mimics Poisson statistics in the sense that the noise image resembles the image itself, although the relationship between image and noise is much more complicated than the Poisson rule $\sigma(n) = \sqrt{n}$ (*13,14*). However, the conclusions obtained below are valid even if the dependence on Poisson statistics is relaxed to proportionality rather than equality between $\sigma(n)$ and $\sqrt{n}$.

Symbols used in the equations are as follows: T, acquisition time used for study; C, counts; R, counting rate; and Q, ventilation/perfusion quotient. Each of the symbols T, C, and R are subscripted by v for the ventilation study, by p for the perfusion study, or by pv for a quotient: $T_{pv} \equiv T_p/T_v$. The symbols C_p and R_p include the remains of the ventilation study as background.

Q is given by the expression:

$$Q = C_v/(C_p - T_{pv}C_v), \qquad \text{Eq. 1}$$

where the different acquisition times for ventilation and perfusion are accounted for by the subtraction of a fraction, T_p/T_v of C_v from C_p. Clearance is not considered in this expression.

The relationship for error propagation for the noncorrelated quantities C_v and C_p is:

$$\sigma^2(Q) = \left(\frac{\partial Q}{\partial C_v}\right)^2 \sigma^2(C_v) + \left(\frac{\partial Q}{\partial C_p}\right)^2 \sigma^2(C_p). \qquad \text{Eq. 2}$$

Insertion of the partial derivatives of Equation 1 with respect to C_v and C_p, into Equation 2, and also using the property of Poisson statistics that $\sigma^2(C) = C$, and finally dividing by Q^2 to obtain the relative variance yields:

$$\frac{\sigma^2(Q)}{Q^2} = \frac{(C_p^2/C_v) + C_p}{(C_p - T_{pv}C_v)^2}. \qquad \text{Eq. 3}$$

Because the limiting conditions are the total time available and the total dose to the patient, we wish to examine Equation 3 in such a form that $(T_v + T_p)$ and R_p are fixed (R_p is by definition the counting rate in the perfusion study, at which time the patient has received both the ventilation and the perfusion activity). Using $C_{pv} \equiv C_p/C_v = (R_pT_p)/(R_vT_v) = R_{pv}T_{pv}$ and extracting the factor $1/([T_v + T_p]R_p)$ yields after some rearrangement:

$$\frac{\sigma^2(Q)}{Q^2} = \frac{1}{(T_v + T_p)R_p} \times \frac{(T_{pv}^{-1} + 1)(R_{pv}T_{pv} + 1)}{(1 - R_{pv}^{-1})^2}. \qquad \text{Eq. 4}$$

The second major factor now contains the only variable quantities. It was mapped numerically to show a shallow minimum in the region of $T_{pv} = 0.5 \pm 0.2$ and $R_{pv} = 4 \pm 1$ (variance increase 5% at ± tolerance). This leads to the rule of thumb that while using one third of the totally available scan time, the counting rate at perfusion should be 4 times that of the ventilation counting rate. It also follows that the tolerances for these values are fairly wide.

Patient Protocol

The finally adopted protocol conforms to the guideline given above, and also, with respect to counting rates and radiopharmaceuticals, to that of the Society of Nuclear Medicine (*15*). On the basis of this and the result of the phantom studies, the following configuration was used for patient studies: low-energy, all-purpose collimator; a 64 × 64 matrix zoomed to a pixel size of 6.8 mm, with 128 projections over 360°. Sixty-four steps of duration 10 s and 5 s were used for ventilation and perfusion studies, respectively. An overview of the entire procedure is given in Figure 1. The proposed activity for ventilation scintigraphy was 30 MBq ^{99m}Tc-DTPA (TechneScan DTPA; Mallinckrodt Medical BV, Petten, Holland) and for perfusion was 100 MBq ^{99m}Tc-labeled macroaggregated albumin (TechneScan LyoMAA; Mallinckrodt Medical BV). Using this protocol the number of counts expected in the ventilation and perfusion study would be 2×10^6 in 12 min and 4×10^6 in 6 min, respectively, so that the counting rate at perfusion is 4 times that of ventilation. The supine patient inhaled the aerosol from a pressurized air-driven nebulizer as described (*16*). Inhalation was terminated when a collimated Geiger-Müller tube monitor over the chest indicated that 30 MBq ^{99m}Tc-DTPA had been deposited in the lungs. The patient was then transferred immediately to the SPECT table and asked to be still in a comfortable supine position. At the completion of ventilation acquisition, the perfusion marker was injected immediately without moving the patient. The perfusion acquisition was then performed.

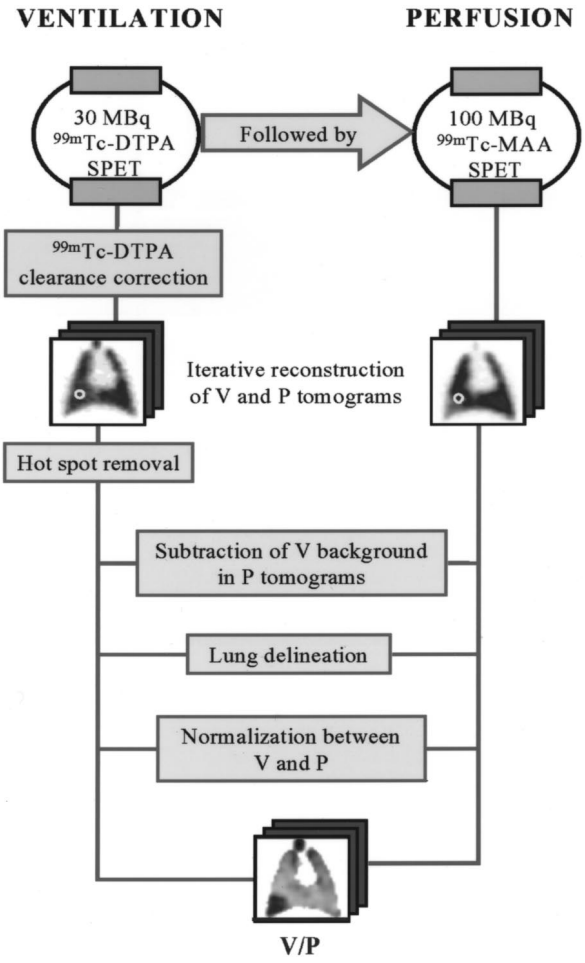

FIGURE 1. Procedure overview. SPET = single photon emission tomography; MAA = macroaggregated albumin.

Raw Data Processing and SPECT Reconstruction

Before reconstruction, the ventilation projections were analyzed to obtain an estimate of lung clearance and to use that estimate to correct the projections for clearance. The first acquired frontal and dorsal projections were added to obtain an initial image, as were the last closely similar projections to obtain a final image. If present, focal aerosol deposition, "hot spots," were then removed from these images with an automatic procedure described below. The lungs were displayed and the lung contour was drawn manually, at a threshold of 25% of the maximum within the individual lung. This procedure facilitated a consistent definition of the lung fields, which in most cases could have been automated. Because of occasional problems with extrapulmonary uptake, and the need to avoid the left heart chamber region, we decided to define the contours manually. The pulmonary half-time for ^{99m}Tc-DTPA was then calculated from the time difference between the 2 first and 2 last projections (11.8 min) and the counts in the initial and final lung fields. The clearance correction was implemented to produce 2 corrected projection sets: 1 assuming constant clearance and 1 allowing variable clearance in the apicobasal direction. The latter was obtained by calculating the clearance on a pixel-by-pixel basis and using the axial component as obtained from multiple linear regressions. Transverse slices were reconstructed using OSEM with 8 subsets and 2 iterations. No filtering was applied as part of the reconstruction process. The resulting multislice set was normalized to contain the same number of voxel counts as the pixel counts contained in the projection set within the applied slice range.

Postreconstruction Processing

Focal deposition of aerosol may result in local counts several times that of the surrounding lung tissue. Therefore, it is essential to remove hot spots before relying on thresholding methods that are defined in relation to a maximum pixel count. Hot spots were removed in 2 contexts: first in the copy of the planar projections used for the clearance calculation and second, 3-dimensionally, in the reconstructed ventilation slice set. The algorithm, in part similar to that of Holst et al. (*17*), worked with 3 images: the original image (Original), a highly smoothed image (Lowpass), and a map of isolated hot spots (Hotspotmap). The latter was constructed after statistical considerations using Original and Lowpass. At completion, the map hot spots have central counts of unity and trail to zero at the edges. The required hot spot–removed image was obtained as Original $\times$ (1 $-$ Hotspotmap) + 0.9 $\times$ Lowpass $\times$ Hotspotmap. At the location of a hot spot it reduces to 0.9 $\times$ Lowpass—that is, a slightly reduced highly smoothed image. At other locations, extraneous to hot spots, Hotspotmap = 0 and the value reduces to Original. The expression thus provides for a seamless transition from the original image to adjusted areas at hot spot locations (Fig. 2).

To account for the remains of aerosol in the perfusion study, the multislice ventilation set was counted down, using the clearance half-life, to the time of the beginning of the perfusion SPECT acquisition and subtracted from the reconstructed multislice perfusion set. Because the background counting rate associated with ventilation is only 20%–30% of the total, the error incurred by neglecting the change in ventilation background during the short time of perfusion SPECT was ignored.

After reconstruction, the multislice sets were filtered before calculation of the V/P quotient—that is, ventilation/(perfusion $-$ k $\times$ ventilation), where k accounts for clearance and differences of acquisition times. We used a 3-dimensional, low-pass Butterworth filter with an order of 5 and a cutoff of 0.6 Nyquist. The overall lung volume for which ventilation/perfusion was calculated was defined to be the volume in which either ventilation or perfusion exceeded 10% of their respective maximum. For the purpose of relative normalization of ventilation to perfusion, the common volume in which both ventilation and perfusion exceeded 50% of their respective maximum was considered to be representative of normal function. Normalization was set so that the average voxel value in this volume would be equal for ventilation and perfusion.

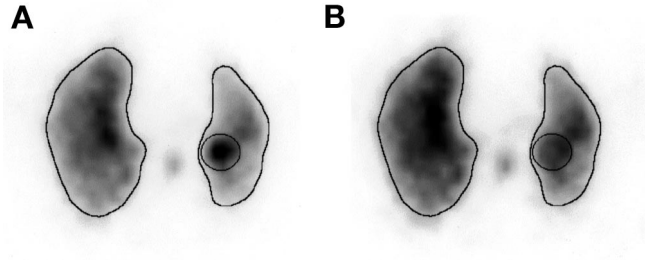

FIGURE 2. Hot spot removal. (A) Transverse slice shows central deposition of aerosol. (B) Transverse slice after automatic hot spot removal.

Patient Selection and Image Interpretation

The study embraces a trial group of 15 clinical patients referred for lung scintigraphy. They were consecutive in the sense that a tomographic study was performed whenever the tomographic camera was available at the time when a patient was referred to us. Accordingly, patient selection was not specific for the purpose of the study. The reasons for referral were to check the early effect of therapy in 3 patients with known lung embolism; for surgery in 1 patient with lung cancer; and clinical symptoms in 11 patients in whom lung embolism was suspected. The final diagnosis, as presented in Table 2, was established by clinicians when the patient left the hospital.

An experienced physician who was unaware of clinical information reviewed, in 2 separate sessions, all planar and SPECT images. In each session the order of the patients was randomized. Ventilation and perfusion defects were graded according to revised Prospective Investigation of Pulmonary Embolism Diagnosis criteria. A segmental reduction or a subsegmental total deficiency was attributed 1 point; a segmental total deficiency was attributed 2 points. In the review of the SPECT images, slices were condensed to 13.6-mm thickness, and the reviewer first described all changes found in sagittal, transverse, and frontal slices of ventilation (V) and perfusion (P). The number of points reflecting a perfusion defect—that is, mismatch implying that $P << V$—were noted. The opposite—that is, reversed mismatch—was also recorded. Then, in the same patient, the V/P quotient slices were displayed together with the V and P slices. As an adjunct to V and P slices, a rotating 3-dimensional display offered synchronized viewing of V, P, and the V/P quotient. The number of mismatch points and reversed mismatch points was reestimated and the V/P quotient, if judged to supply additional information, was classified as supportive or important for the evaluation (Table 2).

RESULTS

Table 1 shows that the number of counts needed to reach a high sensitivity in the detection of defects is in the range $3–5 \times 10^6$ counts. The highest performance was obtained in a 128×128 matrix with the high-resolution collimator. However, the sensitivity of this collimator is half that of the all-purpose collimator, requiring twice the amount of acquisition time for the same number of counts. With the all-purpose collimator, the 128×128 matrix did not offer any advantage. Accordingly, the all-purpose collimator and the 64×64 matrix were used for the patient studies. In the patient studies, the ventilation and perfusion yielded 1.8 ± 0.4 and 3.8 ± 0.7 million counts, respectively. This was within the a priori range estimated to provide optimal imaging considering restrictions in dose and acquisition time. The visual quality of the images was judged adequate for diagnostic purposes (Figs. 3–5). The images for all 15 patients were scrutinized for signs of misalignment, but no such case was encountered. The median estimated half-time for ^{99m}Tc-DTPA in the lungs was 49 min (range, 27–140 min). The counts obtained during the short time of acquisition allowed the half-time to be determined with an accuracy of about 10%. For the patient studied with the shortest half-time, the reduction in counts during the 11.8 min of acquisition resulted in a correction of 35% for the final pair of images. In terms of relative variation within reconstructed ventilation images, the effect of correction was in the range ±7%. It was impossible to visually distinguish between corrected and noncorrected reconstructed images.

Planar imaging showed 12 mismatch points, classified as embolism, in 1 patient (patient 8) and 2 mismatch points, classified as suspected embolism, in 1 patient (patient 11) (Table 2). Ventilation and perfusion tomography showed 12 mismatch points in both of these patients. Figure 3 illustrates planar and tomographic images of patient 11. One additional patient (patient 2) showed 4 mismatch points on

TABLE 2
Patient Symptom or Diagnosis and Scintigraphic Findings

Patient no.	Symptom or diagnosis	Planar		Tomography		V/P quotient (mmp)	Comment to tomography
		mmp	r-mmp	mmp	r-mmp		
1	Cancer (pulmonary), COPD, BS	0	3	0	8	S	COPD
2	Lung embolism, LE	0	3	4	0	I (7)	LE
3	COPD, SE	0	5	0	9	S	COPD
4	Recurrent pneumonia, SE	0	0	0	0		N
5	Myocardial infarction, incompensation, SE	0	3	0	6	I	Incomp COPD
6	Hemoptysis, SE	0	3	0	2	S	Incomp
7	Angina, dyspnea, SE	0	0	0	0		N
8	Lung embolism, LE	12	0	12	0	S (14)	LE
9	Angina, SE	0	0	0	0		N
10	Wegener's granulomatosis, SE	0	0	0	1		Incomp
11	Lung embolism, LE	2	0	12	0	S	LE
12	Angina, SE	0	0	0	0	S	N
13	Angina, fever, SE	0	2	0	4	S	Incomp
14	Tachycardia, dyspnea, SE	0	3	0	2	S	Incomp?
15	Dyspnea, SE	0	0	0	0		N

mmp = mismatch points; r-mmp = reversal-mismatch points; COPD = chronic obstructive pulmonary disease; BS = before surgery; S = supportive; LE = known embolism; I = important; SE = suspected embolism; N = normal; Incomp = heart incompensation.

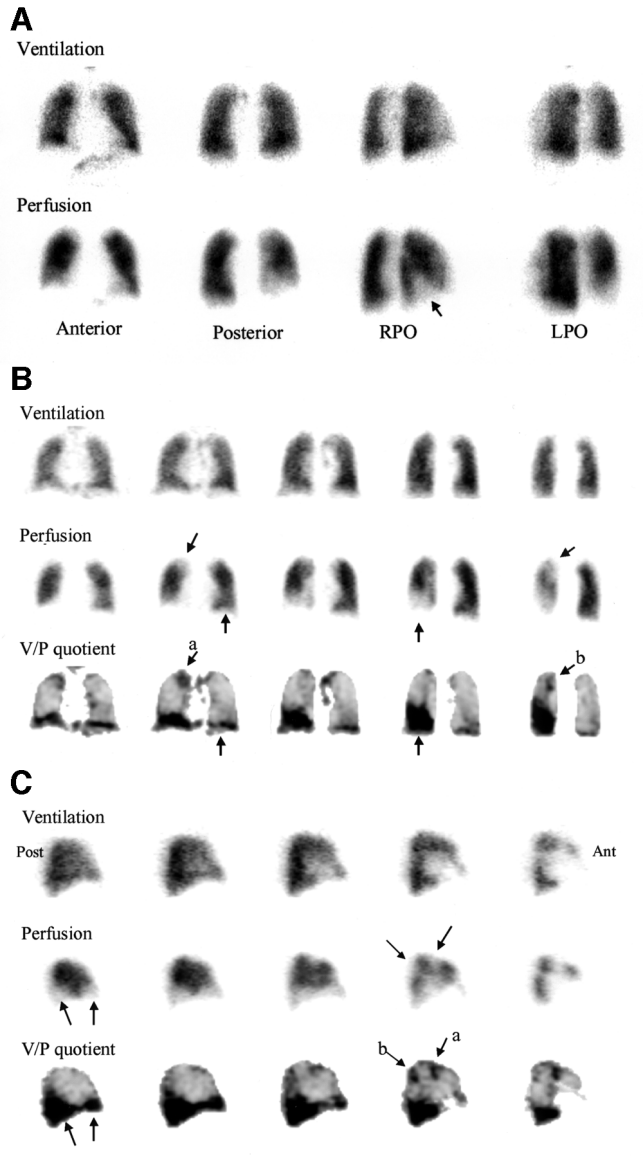

FIGURE 3. Patient 11. (A) Planar images. Basal perfusion defect in right lung is well delineated. RPO = right posterior oblique; LPO = left posterior oblique. (B) Tomograms. Large basal perfusion defect is clearly visible on frontal slices from anterior to posterior even without display of V/P quotient. A smaller basal defect is also seen in left lung. Detection of small perfusion defects is enhanced by V/P quotient (a, b). (C) Sagittal slices of right lung, from lateral to medial. These clarify location of small mismatches (a, b) on V/P quotient images. Post = posterior; Ant = anterior.

tomography; diagnosis was not made from the planar images because of chronic obstructive pulmonary disease (COPD) (Fig. 4). V/P quotient presentation increased the number of mismatch points in 2 of these patients (patients 2 and 8). It was revealed retrospectively that all 3 of these patients were referred for follow-up of known embolism, 24–48 h after thrombolytic therapy. The reversal mismatches were also more unambiguously described on tomographic images. Tomographic images of 5 patients showed a distribution pattern suggesting left heart failure (Fig. 5), which could be perceived in only 2 patients on planar studies. The V/P quotient was supportive in 8 patients and important for diagnosis in 3. In 4 patients, a normal distribution of activity was observed with both modalities (Table 2). For interpretation, the sagittal and frontal slices, the V/P quotient, and the 3-dimensional rendering of the quotient were found to be the most informative.

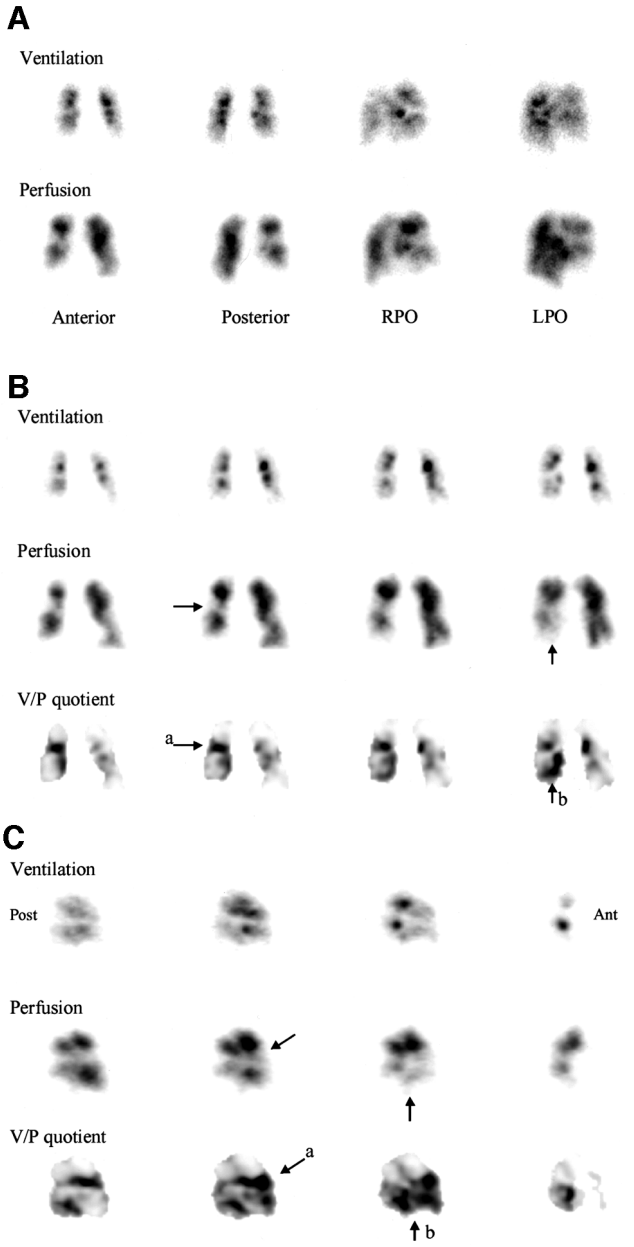

FIGURE 4. Patient 2. (A) Planar images. Ventilation: central deposition of aerosol. Perfusion appears to match ventilation. RPO = right posterior oblique; LPO = left posterior oblique. (B) Tomograms. Perfusion defects are visible on frontal slices but fact that these are mismatches is apparent only from V/P quotient (a, b). (C) Sagittal slices clarify location and extension of mismatches (a, b) on V/P quotient images. Post = posterior; Ant = anterior.

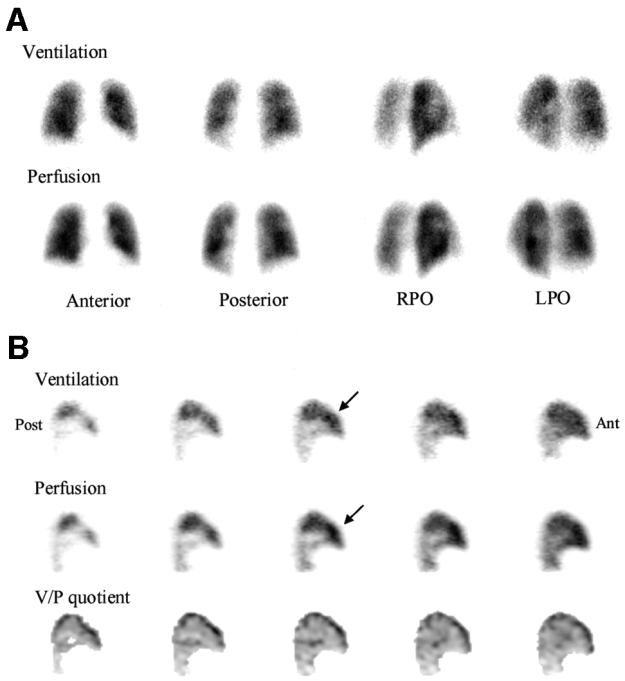

FIGURE 5. Patient 10. (A) Planar images. Inhomogeneous distribution of activity on ventilation and perfusion images. RPO = right posterior oblique; LPO = left posterior oblique. (B) Tomograms. Ventilation and perfusion show clear redistribution on sagittal slices from basal and posterior region to apical and anterior region (arrows), typical for heart incompensation. Post = posterior; Ant = anterior.

DISCUSSION

Methodologic development has led to a feasible clinical routine for ventilation/perfusion tomography. Using a dual-head gamma camera and a protocol based on a total acquisition time of 20 min, the overall gamma-camera time is 30 min for ventilation and perfusion tomography. Examination in the supine position is comfortable for patients and convenient for the staff. Some elderly and critically ill patients can be studied only in the supine position. The administered activity for ventilation and perfusion is in line with the recommendation proposed by the Society of Nuclear Medicine (*15*) and was not changed from that of our routine planar method. It might be hypothesized that a high-resolution collimator and 128 × 128 matrix should be superior to our choice of an all-purpose collimator and 64 × 64 matrix. However, the limitations imposed by patient dose and patient acquisition time imply that the total counts, using the all-purpose collimator, are in the range 1.5–2.5 × 10^6 for the ventilation study and in the range 3–5 × 10^6 for the perfusion study. If the high-resolution collimator had been used, these values would be approximately halved. It can be seen from Table 1 that, at these lower count levels, there is no advantage in the use of a high-resolution collimator or of 128 × 128 matrix slices. In addition, the storage space required is 8-fold over that for 64 × 64 matrix slices, which would also considerably complicate processing and archiving. More detailed images with a high-resolution collimator and 128 ×128 matrix would take about twice the acquisition time or twice as large a dose. The longer acquisition is judged too costly and too uncomfortable for the patient. Patient movements might then jeopardize the enhancement in quality. We consider that a higher dose would not be justified ethically by an increased image quality of doubtful clinical significance. The use of ^{99m}Tc-DTPA aerosol allows determination of alveolocapillary clearance as an indicator of alveolar inflammatory disease (*18*). It also has implications for SPECT imaging. The effect of correcting ventilation projections for clearance before reconstruction was measurable but not dramatic. Typically, clearance over the ventilation acquisition time span will cause a counting rate change of 10%–40%. We consider correction appropriate because clearance of this magnitude led to measurable effects in reconstruction. A further aspect is that clearance might be inhomogeneous. It is within the capability of the method to correct for differential clearance in the tomographic axial direction (base to apex of the lungs) but not in the transverse direction. An extension of the clearance correction to include an apex-to-base gradient gave only small effects and was judged not to have merit in this material. Patient immobilization is critical for accurate calculation of ratio images. However, artifacts caused by patient motion between ventilation and perfusion are usually readily identifiable. Image relocation procedures were not applied in this study but could be considered in a fully developed application of the method. Attenuation is not an issue in the V/P quotient because the effects were similar in the 2 immediately succeeding SPECT studies of the same patient. Quotient images appear to have an obvious application in assessment of image mismatch but have not been commonly used in lung scintigraphy. SPECT quotient images, and numeric indices, of the alveolar gaseous exchange/perfusion match in SPECT were obtained by Sando et al. (*19*) using ^{81m}Kr and ^{99m}Tc-MAA simultaneously, with appropriate cross-talk correction. The technique yields scientifically interesting results but, because of cost and availability, is probably not suitable for routine scintigraphy. A drawback is the limited spatial resolution because of the need to use a medium-energy collimator. Holst et al. (*17*) obtained inputs for neural networks from planar quotient images by an automatic procedure but did not use the quotient images as a primary visual aid. The networks performed well, giving a receiver operating characteristic curve area of 0.79 in a test group. It is conceivable to extend the method to SPECT images, although the data reduction necessary for network input may defy the purpose of SPECT, which is to increase the information content of the study. Networks need large training databases and these are not currently available for lung SPECT.

Among patients referred to us for lung scintigraphy, obstructive and other lung diseases, heart failure, and cancer are together more prevalent than embolism. Although small, our group of 15 patients appears representative. Tomo-

graphic images provide clearer ventilation and perfusion data compared with planar images and were judged to be more conclusive. The number of mismatched points and reversal-mismatched points was considerably higher with tomography (Table 2). In cardiac failure, an offset or even reversed gravitational perfusion and ventilation gradient is well known (*20*). In this study, such signs were much more evident on tomographic images than on planar images (Fig. 5). For the final diagnosis, V/P quotient images were judged to be supportive in most cases and even crucial in some. In this limited group of patients, the results indicate a large potential for tomography in clinical routine because tomography allows improved classification of various diseases.

Lung scintigraphy is proposed as a first choice in decision making for patients with suspected lung emboli (*11*,*21*) and is still the most frequently used method (*22*). However, it can easily lose priority, particularly with respect to spiral CT. Some studies indicate that spiral CT has a higher sensitivity and specificity for the diagnosis of central lung embolism (*11*,*12*). However, the sensitivity for subsegmental embolism is low for spiral CT (*7*). A recent review concludes that the use of spiral CT in the diagnosis of pulmonary embolism has not been adequately evaluated (*23*). This study supports the results from earlier studies showing that scintigraphic tomography significantly improves the detectability and characterization of defects in patients and phantoms (*8*,*10*,*24*). Conventional planar scintigraphy, which requires similar patient and health care commitment, does not extract all of the useful diagnostic information. We show the feasibility of fast, high-quality, ventilation and perfusion imaging with standard isotope doses. Further discussions about spiral CT and scintigraphy should be based on studies made with techniques that are up to date for both methods.

CONCLUSION

High-quality ventilation/perfusion tomography was shown to be feasible for routine use with the examination time of about 30 min for ventilation/perfusion tomography. This study supports the results from earlier studies showing that scintigraphic tomography significantly improves the detectability and characterization of defects in the patients. The V/P quotient used as an objective indicator was important, particularly in the patients with COPD. The method may contribute to higher objectivity in evaluating lung embolism as well as other lung diseases. The costs for the procedure and patient care until diagnosis are low because of the comprehensive system for the study and, particularly, the short time for its completion.

ACKNOWLEDGMENT

This study was supported by the Swedish Heart Lung Foundation and the Swedish Medical Research Council (grant 02872).

REFERENCES

1. Morell TM, Truelove SC, Barr A. Pulmonary embolism. *Br Med J*. 1963;2:830–835.
2. Alpert JS, Smith R, Carson CJ, et al. Mortality in patients treated for pulmonary embolism. *JAMA*. 1976;13:1477–1480.
3. Carson JL, Kelly MA, Duff A, et al. The clinical course of pulmonary embolism. *N Eng J Med*. 1992;19:1240–1245.
4. Opinions regarding the diagnosis and management of venous thromboembolic disease: ACCP Consensus Committee on Pulmonary Embolism—American College of Chest Physicians. *Chest*. 1998;113:499–504.
5. Gottschalk A, Juni JE, Sostman HD, et al. Ventilation-perfusion scintigraphy in the PIOPED study. Part 1. Data collection and tabulation. *J Nucl Med*. 1993;34:1109–1118.
6. Gottschalk A, Sostman HD, Coleman RE, et al. Ventilation-perfusion scintigraphy in the PIOPED study. Part 2. Evaluation of the scintigraphic criteria and interpretations. *J Nucl Med*. 1993;34:1119–1126.
7. Woodard PK. Pulmonary arteries must be seen before they can be assessed [editorial]. *Radiology*. 1997;204:11–12.
8. Corbus HF, Seitz JP, Larson RK, et al. Diagnostic usefulness of lung SPET in pulmonary thromboembolism: an outcome study. *Nucl Med Commun*. 1997;18:897–906.
9. Eustace S, Phelan N, Dowsett DJ, Ennis JT. A comparison of SPECT and planar ventilation perfusion lung scanning. *Ir J Med Sci*. 1993;162:82–85.
10. Magnussen JS, Chicco P, Palmer AW, et al. Single photon emission tomography of a computerized model of pulmonary embolism. *Eur J Nucl Med*. 1999;26:1430–1438.
11. Maki DD, Gefter WB, Alavi A. Recent advances in pulmonary imaging. *Chest*. 1999;116:1388–1402.
12. Kim KI, Muller NL, Mayo JR. Clinically suspected pulmonary embolism: utility of spiral CT. *Radiology*. 1999;210:693–697.
13. Barrett HH, Wilson DW, Tsui BMW. Noise properties of the EM algorithm. I. Theory. *Phys Med Biol*. 1994;39:833–846.
14. Wilson DW, Tsui BMW, Barrett HH. Noise properties of the EM algorithm. II. Monte Carlo simulations. *Phys Med Biol*. 1994;39:847–871.
15. Society of Nuclear Medicine. *Procedure Guidelines*. Reston, VA: Society of Nuclear Medicine; 1999.
16. Tägil K, Evander E, Wollmer P, Palmer J, Jonson J. Efficient lung scintigraphy. *Clin Physiol*. 2000;20:95–100.
17. Holst H, Åström K, Järund A, et al. Automated interpretation of ventilation-perfusion lung scintigrams for the diagnosis of pulmonary embolism using artificial neural networks. *Eur J Nucl Med*. 2000;27:400–406.
18. Rindernknecht J, Sharpio L, Krauthammer M, et al. Accelerated clearance of small solutes from the lungs in interstitial disease. *Am Rev Respir Dis*. 1989;121:105–117.
19. Sando Y, Inoue T, Nagai R, Endo K. Ventilation/perfusion ratios and simultaneous dual-radionuclide single-photon emission tomography with krypton-81m and technetium-99m macroaggregated albumin. *Eur J Nucl Med*. 1997;24:1237–1244.
20. Speziale G, De Biase L, De Vincentis G, et al. Inhaled nitric oxide in patients with severe heart failure: changes in lung perfusion and ventilation detected using scintigraphy. *Thorac Cardiovasc Surg*. 1996;44:35–39.
21. Robinson PJA. Ventilation-perfusion lung scanning and spiral computed tomography of the lungs: competing or complementary modalities? *Eur J Nucl Med*. 1996;23:1547–1553.
22. Burkill GJ, Bell JR, Padley SP. Survey on the use of pulmonary scintigraphy, spiral CT and conventional pulmonary angiography for suspected pulmonary embolism in the British Isles. *Clin Radiol*. 1999;54:807–810.
23. Rathbun SW, Raskob GE, Whitsett TL. Sensitivity and specificity of helical computed tomography in the diagnosis of pulmonary embolism: a systematic review. *Ann Intern Med*. 2000;132:227–232.
24. Palla A, Tumeh SS, Nagel JS, et al. Detection of pulmonary perfusion defects by single photon emission computed tomography. *J Nucl Med Allied Sci*. 1988;32:27–32.

JNM The Journal of NUCLEAR MEDICINE

Comprehensive Ventilation/Perfusion SPECT

John Palmer, Ulrika Bitzén, Björn Jonson and Marika Bajc

J Nucl Med. 2001;42:1288-1294.

The Journal of Nuclear Medicine is published monthly.
SNMMI | Society of Nuclear Medicine and Molecular Imaging
1850 Samuel Morse Drive, Reston, VA 20190.
(Print ISSN: 0161-5505, Online ISSN: 2159-662X)

SNMMI SOCIETY OF NUCLEAR MEDICINE AND MOLECULAR IMAGING